THE EUROPEAN
PHYSICAL JOURNAL C

Regular Article - Theoretical Physics

Shadows and photon spheres with spherical accretions in the four-dimensional Gauss–Bonnet black hole

Xiao-Xiong Zeng[1,2,a], **Hai-Qing Zhang**[3,4,b] (iD), **Hongbao Zhang**[5,6,c]

[1] State Key Laboratory of Mountain Bridge and Tunnel Engineering, Chongqing Jiaotong University, Chongqing 400074, China
[2] Department of Mechanics, Chongqing Jiaotong University, Chongqing 400074, China
[3] Department of Space Science, Center for Gravitational Physics, Beihang University, Beijing 100191, China
[4] International Research Institute for Multidisciplinary Science, Beihang University, Beijing 100191, China
[5] Department of Physics, Beijing Normal University, Beijing 100875, China
[6] Theoretische Natuurkunde, Vrije Universiteit Brussel, and The International Solvay Institutes, Pleinlaan 2, 1050 Brussels, Belgium

Abstract We investigate the shadows and photon spheres of the four-dimensional Gauss–Bonnet black hole with the static and infalling spherical accretions. We show that, for both cases, there always exist shadows and photon spheres. The radii of the shadows and photon spheres are independent of the profiles of accretion for a fixed Gauss–Bonnet constant, implying that the shadow is a signature of the spacetime geometry and it is hardly influenced by accretion. Because of the Doppler effect, the shadows of the infalling accretion are found to be darker than in the static case. We also investigate the effect of the Gauss–Bonnet constant on the shadow and photon spheres, and we find that the larger the Gauss–Bonnet constant is, the smaller the radii of the shadow and photon spheres will be. In particular, the observed specific intensity increases as the Gauss–Bonnet constant grows.

1 Introduction

The Event Horizon Telescope (EHT) Collaboration has recently obtained an ultra high angular resolution image of the accretion flow around the supermassive black hole in M87* [1–6]. The image shows that there is a dark interior with a bright ring surrounding it. The dark interior is called a black hole shadow while the bright ring is called a photon ring. The shadow of a black hole is caused by gravitational light deflection [7–11]. Specifically, when light emitting from the accretion passes through the vicinity of the black hole toward the observer, its trajectory will be deflected. The intensity of the light observed by the distant observer dif-

fers accordingly, leading to a dark interior and bright ring. So far, the shadows of various black holes have been investigated. It is generally known that the shadows of spherically symmetric black holes are round and those of rotating black holes are not precisely round but deformed.

Since the release of the image and data by EHT, its various implications have been explored. For instance, the extra dimensions could be determined from the shadow of M87* [12,13], where a rotating braneworld black hole was considered. The shadows of high-redshift supermassive black holes may serve as the standard rulers [14], whereby the cosmological parameters can be constrained. The black hole companion for M87* can also be constrained through the image released by EHT [15]. Moreover, the information given by EHT can be used to impose constraints on particle physics via the mechanism of superradiance [16,17]. In particular, for the vector boson, it may constrain some of the fuzzy dark matter parameter space. In addition, dense axion cloud can also be induced by rapidly rotating black holes through superradiance [18].

Accretion matter is apparently important for the shadows of black holes, since many astrophysical black holes are believed to be surrounded by accretion matter. The first image of a black hole surrounded by thin disk accretion was presented in [19]. For a geometrically and optically thick accretion disk [20], it was found that the mass of the disk would affect the shadow of the black hole, and as the mass grows the shadow becomes more prolate. In particular, by reanalyzing the trajectory of the light ray, the shadows of a Schwarzschild black hole with both thin and thick accretion disks have been clarified and detailed recently [21]. It was

[a] e-mail: xxzengphysics@163.com

[b] e-mail: hqzhang@buaa.edu.cn (corresponding author)

[c] e-mail: hzhang@vub.ac.be

found that there existed not only the photon ring[1] but also the lensing ring. The lensing ring makes a significant contribution to the observed flux while the photon ring makes a little contribution. In addition, the observed size of the central dark area was found to be determined not only by the gravitational redshift but also by the emission profile. When the accretion matter is spherically symmetric, there is also a shadow for the black hole [23]. The location of the shadow edge is found to be independent of the inner radius at which the accreting gas stops radiating [22]. The size of the observed shadow can serve as a signature of the spacetime geometry, since it is hardly influenced by the details of the accretion. This result is different from the case in which the accretion is a disk [21].

In this paper, we intend to investigate the shadow of a four-dimensional Gauss–Bonnet black hole with spherical accretions [24]. The Gauss–Bonnet term in the Lagrangian is topologically invariant in four-dimensional spacetime. Thus in order to consider the dynamical effect of Gauss–Bonnet gravity, one is generically required to work in higher dimensions [25,26]. Very recently, Glavan and Lin have proposed Gauss–Bonnet modified gravity in four dimensions by simply rescaling the Gauss–Bonnet coupling constant $\alpha \rightarrow \alpha/(D-4)$ and taking the limit $D \rightarrow 4$ [24]. However, as many authors have pointed out, this theory is not well-defined with the initial regularization scheme [27–30]. Recently, the authors in [31] have proposed a consistent theory of four-dimensional Gauss–Bonnet gravity using the ADM decomposition of the spacetime. They successfully found a four-dimensional Gauss–Bonnet theory of two dynamical degrees of freedom by breaking the temporal diffeomorphism invariance. Thus, the cosmological and black hole solutions naively given in [24] can be accounted as exact solutions in the theory of [31]. Our background of the black hole solution indeed also satisfies the well-defined theory of [31]. Many other characteristics of the four-dimensional Gauss–Bonnet black hole have been investigated; see for instance [32–47].

In particular, gravitational lensing by black holes in ordinary medium and homogeneous plasma in four-dimensional Gauss–Bonnet gravity have been studied in [48,49]. The shadows cast by the spherically symmetric [32,50] and rotating [51] four-dimensional Gauss–Bonnet black hole have also been studied. It will be more interesting to investigate the corresponding light intensity of the shadow, which comprises the main issue of this paper. To be more precise, in this paper, we are interested in spherical accretions, which can be classified into static and infalling. On the one hand, we want to explore how the Gauss–Bonnet constant affects the radii of the shadow and photon sphere as well as the light inten-

sity observed by a distant observer. On the other hand, we want to explore how the dynamics of the accretion affects the shadow of the black hole. As a result, we find that the larger the Gauss–Bonnet constant is, the smaller the radii of the shadow and photon sphere will be, and the larger the intensity will be. In addition, the shadow of the infalling accretion are found to be darker than that of the static case because of the Doppler effect.

The remainder of this paper is organized as follows. In Sect. 2, we investigate the motion of the light ray near the four-dimensional Gauss–Bonnet black hole and figure out how it is deflected. In Sect. 3, we investigate the shadows and photon spheres with the static spherical accretion. To explore whether the dynamics of the accretion will affect the shadow and photon sphere, the accretion is supposed to be infalling in Sect. 4. Section 5 is devoted to the conclusions and discussions. Throughout this paper, we set $G = \hbar = c = k_B = 1$.

2 Light deflection in the four-dimensional Gauss–Bonnet black hole

Starting from the following Einstein–Hilbert action with an additional Gauss–Bonnet term:

$$
I = \frac{1}{16\pi G} \int \sqrt{-g}\mathrm{d}^4x
$$
$$
\times \left[R + \alpha(R_{\mu\nu\lambda\delta}R^{\mu\nu\lambda\delta} - 4R_{\mu\nu}R^{\mu\nu} + R^2) \right], \quad (1)
$$

by rescaling the Gauss–Bonnet coupling constant $\alpha \rightarrow \alpha/(D-4)$ and taking the limit $D \rightarrow 4$, one can obtain the four-dimensional spherically symmetric Gauss–Bonnet black hole:

$$
\mathrm{d}s^2 = -F(r)\mathrm{d}t^2 + \frac{\mathrm{d}r^2}{F(r)} + r^2(\mathrm{d}\theta^2 + \sin^2\theta\mathrm{d}\phi^2), \quad (2)
$$

with

$$
F(r) = 1 + \frac{r^2}{2\alpha}\left(1 - \sqrt{1 + \frac{8\alpha M}{r^3}}\right), \quad (3)
$$

where M is the mass of the black hole. Note that the same solution was already found previously in [52] by considering the Einstein gravity with Weyl anomaly. Solving the equation $F(r) = 0$, one can obtain two solutions,

$$
r_\pm = M \pm \sqrt{M^2 - \alpha}, \quad (4)
$$

in which r_+ and r_- correspond to the outer horizon (event horizon) and inner horizon, respectively. In order to ensure the existence of a horizon, the Gauss–Bonnet coupling constant should be restricted in the range $-8 \leq \alpha/M^2 \leq 1$. For the case $\alpha > 0$ there are two horizons, while for the case $\alpha < 0$ there is only one single horizon.

---

[1] Note that in this paper, the photon ring is defined by the light ray that intersects the plane of the disk three or more times, which is different from other references such as Ref. [22]. To distinguish them, we call the photon ring in Ref. [22] the photon sphere in this paper.

Table 1 The radius r_{ph}, impact parameter b_{ph} of the photon sphere and the event horizon r_+ for different α with $M = 1$

	$\alpha = -7.7$	$\alpha = -5.5$	$\alpha = -3.3$	$\alpha = -1.1$	$\alpha = 0.111$	$\alpha = 0.333$	$\alpha = 0.555$	$\alpha = 0.777$
r_{ph}	4.70134	4.36744	3.95844	3.40373	2.94939	2.83932	2.71357	2.56483
b_{ph}	6.7815	6.46004	6.07084	5.55557	5.15252	5.05903	4.95501	4.83671
r_+	3.94958	3.54951	3.07364	2.44914	1.94287	1.8167	1.66708	1.47223

In order to investigate the light deflection caused by the four-dimensional Gauss–Bonnet black hole, we need to find how the light ray moves around the black hole. As is well known, the light ray satisfies the geodesic equation, which can be encapsulated in the following Euler–Lagrange equation:

$$\frac{d}{d\lambda}\left(\frac{\partial \mathcal{L}}{\partial \dot{x}^\mu}\right) = \frac{\partial \mathcal{L}}{\partial x^\mu}, \tag{5}$$

with λ the affine parameter, $\dot{x}^\mu$ the four-velocity of the light ray and $\mathcal{L}$ the Lagrangian, taking the form

$$\mathcal{L} = \frac{1}{2}g_{\mu\nu}\dot{x}^\mu\dot{x}^\nu$$
$$= \frac{1}{2}\left(-F(r)\dot{t}^2 + \frac{\dot{r}^2}{F(r)} + r^2\left(\dot{\theta}^2 + \sin^2\theta\,\dot{\phi}^2\right)\right). \tag{6}$$

As in [7–9], we focus on the light ray that moves on the equatorial plane, i.e., $\theta = \frac{\pi}{2}$ and $\dot{\theta} = 0$. In addition, since none of the metric coefficients depends explicitly on time t and azimuthal angle ϕ, there are two corresponding conserved quantities, E and L. Combining Eqs. (3), (5) and (6) together, the time, azimuthal and radial component of the four-velocity can be expressed as

$$\dot{t} = \frac{1}{b\left[1 + \frac{r^2}{2\alpha}\left(1 - \sqrt{1 + \frac{8\alpha M}{r^3}}\right)\right]}, \tag{7}$$

$$\dot{\phi} = \pm\frac{1}{r^2}, \tag{8}$$

$$\dot{r}^2 + \frac{1}{r^2}\left[1 + \frac{r^2}{2\alpha}\left(1 - \sqrt{1 + \frac{8\alpha M}{r^3}}\right)\right] = \frac{1}{b^2}, \tag{9}$$

where we have redefined the affine parameter $\lambda \to \lambda/|L|$, and $b = \frac{|L|}{E}$, which is called the impact parameter. The $+$ and $-$ in Eq. (8) correspond to the light ray traveling in the counterclockwise and clockwise along azimuthal direction, respectively. Equation (9) can also be rewritten as

$$\dot{r}^2 + V(r) = \frac{1}{b^2}, \tag{10}$$

where

$$V(r) = \frac{1}{r^2}\left[1 + \frac{r^2}{2\alpha}\left(1 - \sqrt{1 + \frac{8\alpha M}{r^3}}\right)\right] \tag{11}$$

is an effective potential. The conditions for the photon sphere orbit are $\dot{r} = 0$ and $\ddot{r} = 0$, which can be translated to

$$V(r) = \frac{1}{b^2}, \quad V'(r) = 0, \tag{12}$$

where the prime $'$ denotes the first derivative with respect to the radial coordinate r. Based on this equation, we can obtain the radius r_{ph} and impact parameter b_{ph} for the photon sphere, which are shown together with the size of the event horizon r_+ in Table 1 for different α. From this table, we can see that the three parameters, i.e., r_{ph}, b_{ph} and r_+ all decrease as α increases.

Here we would like to take $\alpha = -5.5, 0.555$ as two examples with the corresponding effective potential depicted in Fig. 1. We can see that at the event horizon the effective potential vanishes. It increases and reaches a maximum at the photon sphere, and then decreases as the light ray moves outwards. As a light ray moves in the radially inward direction, the effective potential will affect its trajectory. In Region 1, the light will encounter the potential barrier and then be reflected back in the outward direction. In Region 2, namely $b = b_{ph}$, the light will asymptotically approach the photon sphere. Since the angular velocity is non-zero, it will revolve around the black hole infinitely many times. In Region 3, the light will continue moving in the inward direction since it does not encounter the potential barrier. Eventually, it will enter the inside of the black hole through the event horizon.

Furthermore, the trajectory of the light ray can be depicted according to the equation of motion. Combining Eqs. (8) and (9), we have

$$\frac{dr}{d\phi} = \pm r^2\sqrt{\frac{1}{b^2} - \frac{1}{r^2}\left[1 + \frac{r^2}{2\alpha}\left(1 - \sqrt{1 + \frac{8\alpha M}{r^3}}\right)\right]}. \tag{13}$$

By setting $u = 1/r$, we can transform (13) into

$$\frac{du}{d\phi} = \sqrt{\frac{1}{b^2} - u^2\left(\frac{1 - \sqrt{8\alpha M u^3 + 1}}{2\alpha u^2} + 1\right)} \equiv G(u). \tag{14}$$

From Eq. (14) we can solve ϕ with respect to u. Employing the ParametricPlot,[2] we can plot the trajectory of the light ray, which is shown in Fig. 2. The black, red and green line

---

[2] In many references, such as in Ref. [22], the ray-tracing code is employed to plot the trajectory of the light ray.
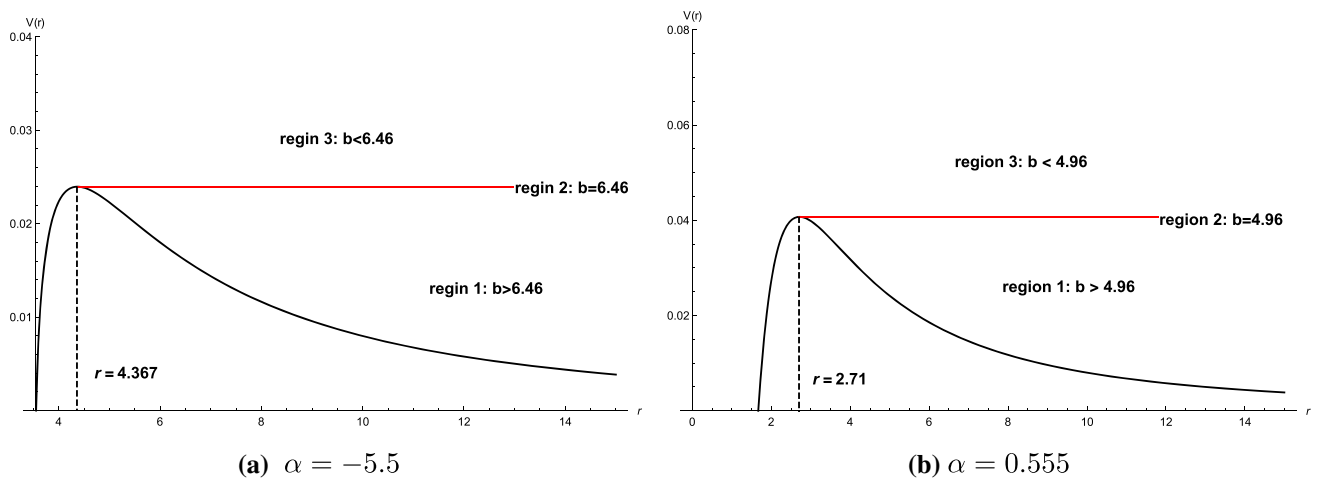
(a) $\alpha = -5.5$

(b) $\alpha = 0.555$

Fig. 1 The profiles of the effective potential for $\alpha = -5.5$ (left panel) and $\alpha = 0.555$ (right panel) with $M = 1$. For both panels, Region 2 corresponds to the red lines where $V(r) = 1/b_{ph}^2$, while Region 1 and Region 3 correspond to $V(r) < 1/b_{ph}^2$ and $V(r) > 1/b_{ph}^2$, respectively
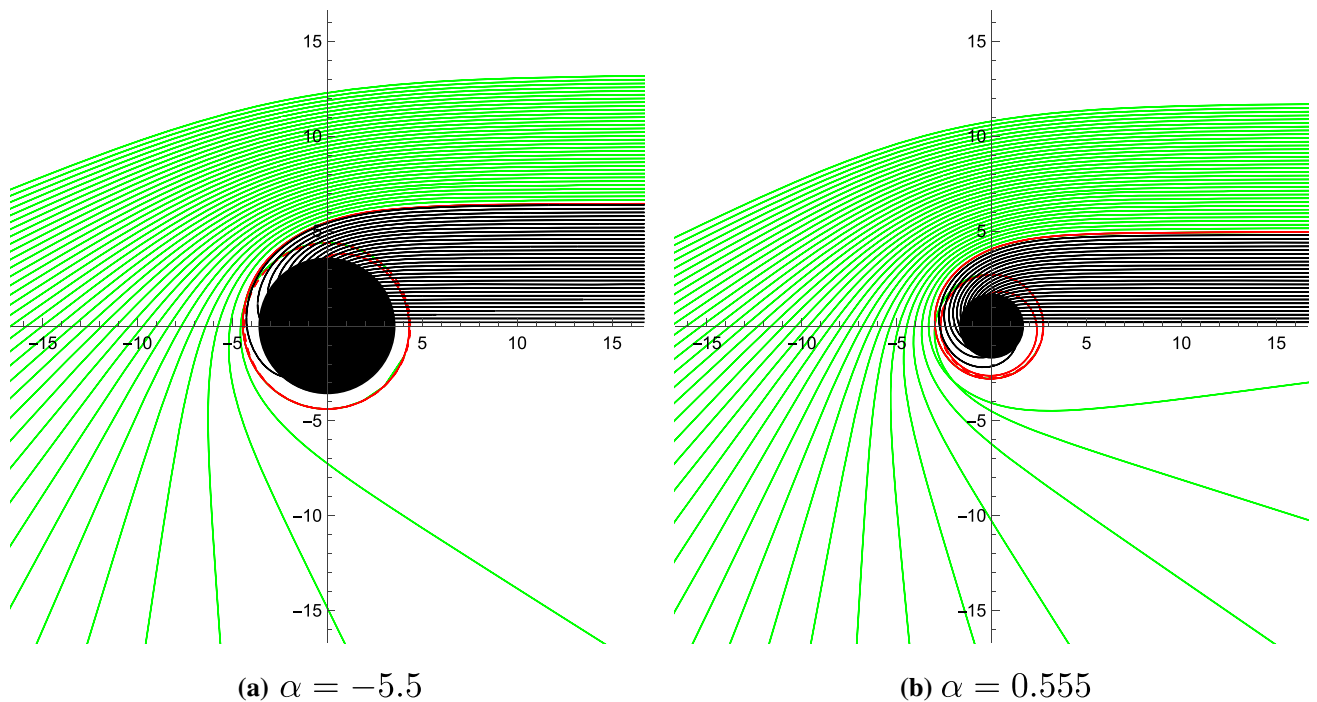

(a) $\alpha = -5.5$

(b) $\alpha = 0.555$

Fig. 2 The trajectory of the light ray for different α with $M = 1$ in the polar coordinates (r, ϕ). The red line corresponds to $b = b_{ph}$, the black line corresponds to $b < b_{ph}$, and the green line corresponds to

$b > b_{ph}$. The spacing in impact parameter is 1/5 for all light rays. The black hole is shown as a solid disk and the photon orbit as a dashed red line

correspond to $b < b_{ph}$, $b = b_{ph}$ and $b > b_{ph}$, respectively. As one can see, for the case of $b < b_{ph}$, the light ray drops all the way into the black hole, which corresponds to Region 3 in Fig. 1. For the case of $b > b_{ph}$, the light ray near the black hole is reflected back, which corresponds to Region 1 in Fig. 1. And for the case of $b < b_{ph}$, the light ray revolves around the black hole, which corresponds to Region 2 in Fig. 1. Note that, for $b > b_{ph}$, in order to plot the geodesic, we should find a turning point, where the light ray changes its radial

direction. The turning point is determined by the equation $G(u) = 0$, where $G(u)$ has been defined in Eq. (14).

3 Shadows and photon spheres with rest spherical accretion

In this section, we will investigate the shadow and photon sphere of the four-dimensional Gauss–Bonnet black hole
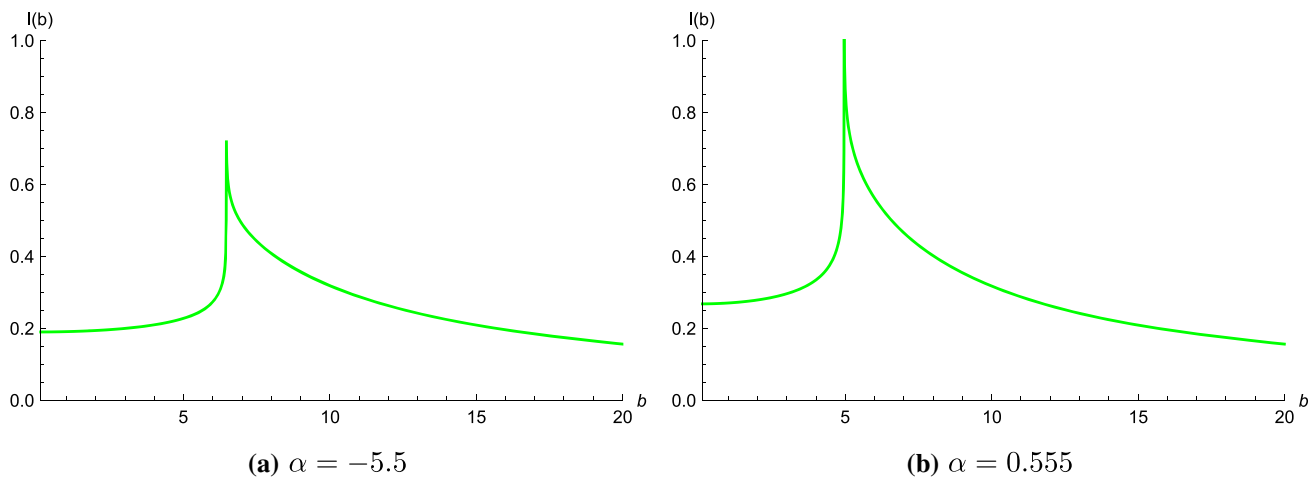
(a) $\alpha = -5.5$

(b) $\alpha = 0.555$

Fig. 3 Profiles of the specific intensity $I(b)$ seen by a distant observer for a static spherical accretion. We set $M = 1$ and take $\alpha = -5.5$ (left panel), and $\alpha = 0.555$ (right panel) as two examples

with static spherical accretion, which is assumed to be optically thin. To this end, we should find the specific intensity observed by the observer (erg s^{-1} cm^{-2} str^{-1} Hz^{-1}). The observed specific intensity I at the observed photon frequency ν_o can be found by integrating the specific emissivity along the photon path [53,54],

$$I(\nu_o) = \int_\gamma g^3 j(\nu_e) dl_{\text{prop}}, \tag{15}$$

where $g = \nu_o/\nu_e$ is the redshift factor, ν_e is the photon frequency of the emitter, dl_{prop} is the infinitesimal proper length, and $j(\nu_e)$ is the emissivity per unit volume measured in the rest frame of the emitter.

In the four-dimensional Gauss–Bonnet black hole, $g = F(r)^{1/2}$. Concerning the specific emissivity, we also assume that it is monochromatic with rest-frame frequency ν_r, that is,

$$j(\nu_e) \propto \frac{\delta(\nu_e - \nu_r)}{r^2}. \tag{16}$$

According to Eq. (2), the proper length measured in the rest frame of the emitter is

$$dl_{\text{prop}} = \sqrt{F(r)^{-1}dr^2 + r^2 d\phi^2}$$
$$= \sqrt{F(r)^{-1} + r^2 \left(\frac{d\phi}{dr}\right)^2} dr, \tag{17}$$

in which $d\phi/dr$ is given by Eq. (13). In this case, the specific intensity observed by the infinite observer is

$$I(\nu_o) = \int_\gamma \frac{F(r)^{3/2}}{r^2} \sqrt{F(r)^{-1} + r^2 \left(\frac{d\phi}{dr}\right)^2} dr. \tag{18}$$

The intensity is circularly symmetric, with the impact parameter b of the radius, which satisfies $b^2 = x^2 + y^2$.

Next we will employ Eq. (18) to investigate the shadow of the four-dimensional Gauss–Bonnet black hole with static spherical accretion. Note that the intensity depends on the trajectory of the light ray, which is determined by the impact parameter b. So we will investigate how the intensity varies with respect to the impact parameter. For different α, the numerical results of $I(b)$ are shown in Fig. 3. From this figure, we see that the intensity increases rapidly and reaches a peak at b_{ph}, and then drops to lower values with increasing b. This result is consistent with Figs. 1 and 2. For $b < b_{ph}$, the intensity originating from the accretion is absorbed mostly by the black hole. And for $b = b_{ph}$, the light ray revolves around the black hole many times, so the observed intensity is maximal. Meanwhile, for $b > b_{ph}$, only the refracted light contributes to the intensity of the observer. As b becomes larger, the refracted light becomes less. The observed intensity thus vanishes for large enough b. In principle, the peak intensity at $b = b_{ph}$ should be infinite because the light ray revolves around the black hole infinite times and collect an arbitrarily large intensity. However, because of the numerical limitations and the logarithmic form of the intensity, the real computed intensity never goes to infinity, which has also been well addressed in [21,22]. From Fig. 3, we can also observe how the Gauss–Bonnet coupling constant affects the observed intensity. For all the b, the larger the coupling constant is, the stronger the intensity will be.

The shadow cast by the four-dimensional Gauss–Bonnet black hole in the (x, y) plane is shown in Fig. 4. We can see that outside the black hole shadow, there is a bright ring, which is the photon sphere. The radii of the photon spheres for different α have been listed in Table 1. Obviously, the results in Fig. 4 are consistent with those in Table 1. That is, the larger the Gauss–Bonnet constant is, the smaller the radius of the photon sphere will be.
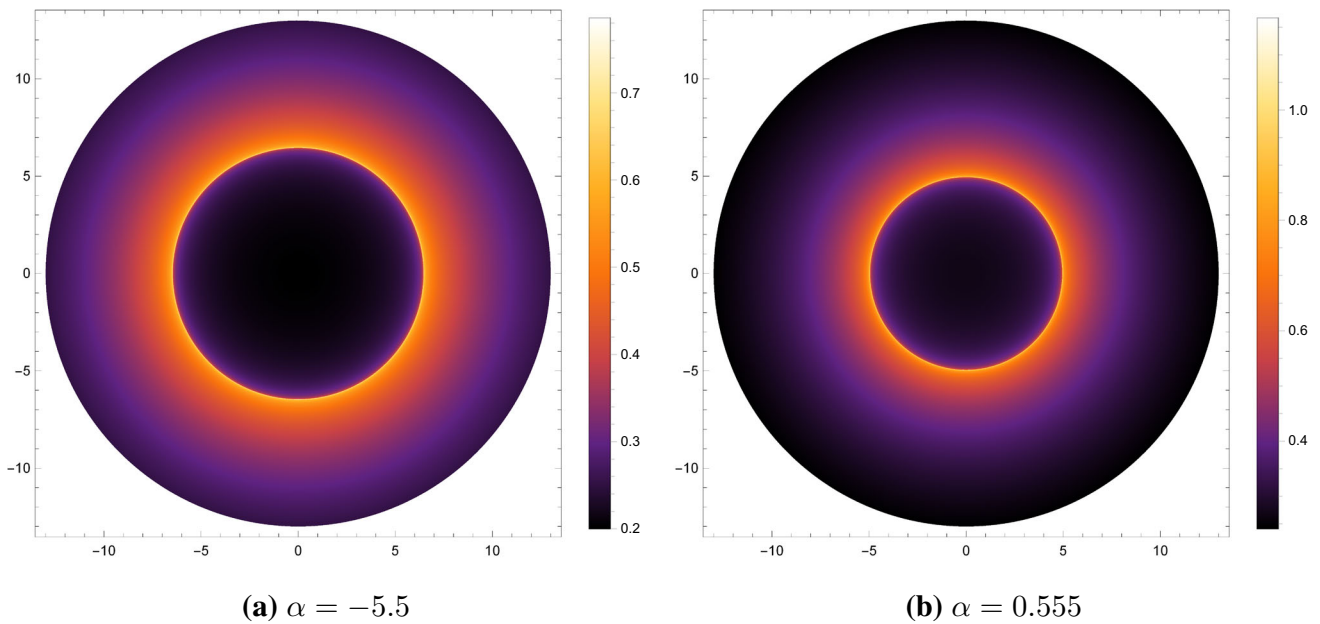
(a) $\alpha = -5.5$

(b) $\alpha = 0.555$

Fig. 4 The black hole shadows cast by static accretion for different α with $M = 1$ in the (x, y) plane. The bright ring is the photon sphere

Table 2 The net luminosity of the escaping rays for different α with $M = 1$

	$\alpha = -7.7$	$\alpha = -5.5$	$\alpha = -3.3$	$\alpha = -1.1$	$\alpha = 0.111$	$\alpha = 0.333$	$\alpha = 0.555$	$\alpha = 0.777$
L_∞	0.169698	0.18729	0.215428	0.265181	0.323863	0.34006	0.359979	0.386447

Moreover, we can see that inside the shadow, the intensity does not go to zero but keeps a small finite value. The reason is that part of the radiation has escaped to infinity. For $r > r_{ph}$, the solid angle of the escaping rays is $2\pi(1+\cos\theta)$, while for $r < r_{ph}$, the solid angle of the escaping rays is $2\pi(1-\cos\theta)$, where θ is given by

$$\sin\theta = \frac{r_{ph}^{3/2}}{r}\left[1 + \frac{r^2}{2\alpha}\left(1 - \sqrt{1 + \frac{8\alpha M}{r^3}}\right)\right]^{1/2}. \quad (19)$$

By only counting the escaping light rays, we have the net luminosity observed at infinity as

$$L_\infty = \int_{r_+}^{r_{ph}} 4\pi r^2 j(\nu_e) 2\pi(1 - \cos\theta)\mathrm{d}r$$
$$+ \int_{r_{ph}}^{\infty} 4\pi r^2 j(\nu_e) 2\pi(1 + \cos\theta)\mathrm{d}r. \quad (20)$$

For different α, the numerical results are listed in Table 2. We can see that the net luminosity increases with increasing α. For the Schwarzschild black hole, the net luminosity is found to be $L_\infty = 0.32$ [22]. Obviously, for the positive α, the net luminosity in the four-dimensional Gauss–Bonnet black hole is larger than that in the Schwarzschild black hole, while for negative α, the net luminosity in this spacetime is smaller than that in Schwarzschild black hole.

4 Shadows and photon spheres with infalling spherical accretion

In this section, we allow the optically thin accretion to move towards the black hole. This model is thought to be more realistic than the static accretion model since most of the accretions are mobile in the universe. For simplicity, we assume that the accretion shows free fall onto the black hole from infinity. We still employ Eq. (18) to investigate the shadow of the four-dimensional Gauss–Bonnet black hole.

Different from the static accretion, the redshift factor for the infalling accretion should be evaluated by

$$g = \frac{k_\beta u_o^\beta}{k_\gamma u_e^\gamma}, \quad (21)$$

in which $k^\mu = \dot{x}_\mu$ is the four-velocity of the photon, $u_o^\mu = (1, 0, 0, 0)$ is the four-velocity of the distant observer, and u_e^μ is the four-velocity of the accretion under consideration, given by

$$u_e^t = \frac{1}{F(r)}, \quad u_e^r = -\sqrt{1 - F(r)}, \quad u_e^\theta = u_e^\phi = 0. \quad (22)$$

The four-velocity of the photon has been obtained previously in Eqs. (7)–(9). We know that $k_t = 1/b$ is a constant, and k_r can be inferred from $k_\gamma k^\gamma = 0$. Therefore,
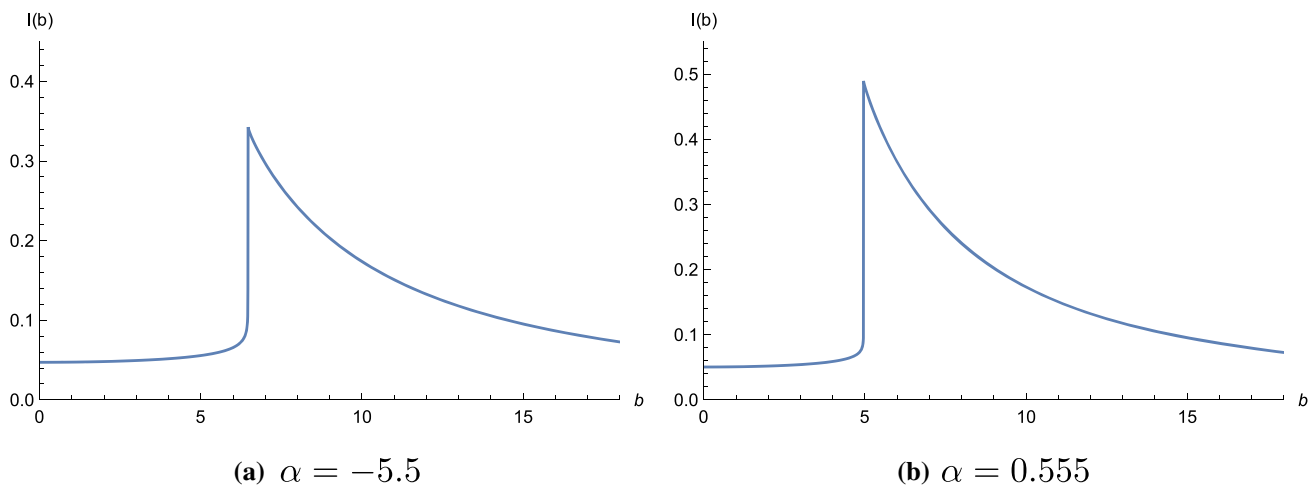
(a) $\alpha = -5.5$ **(b)** $\alpha = 0.555$

Fig. 5 The profiles of the specific intensity $I(b)$ seen by a distant observer for an infalling accretion. For both cases, we set $M = 1$

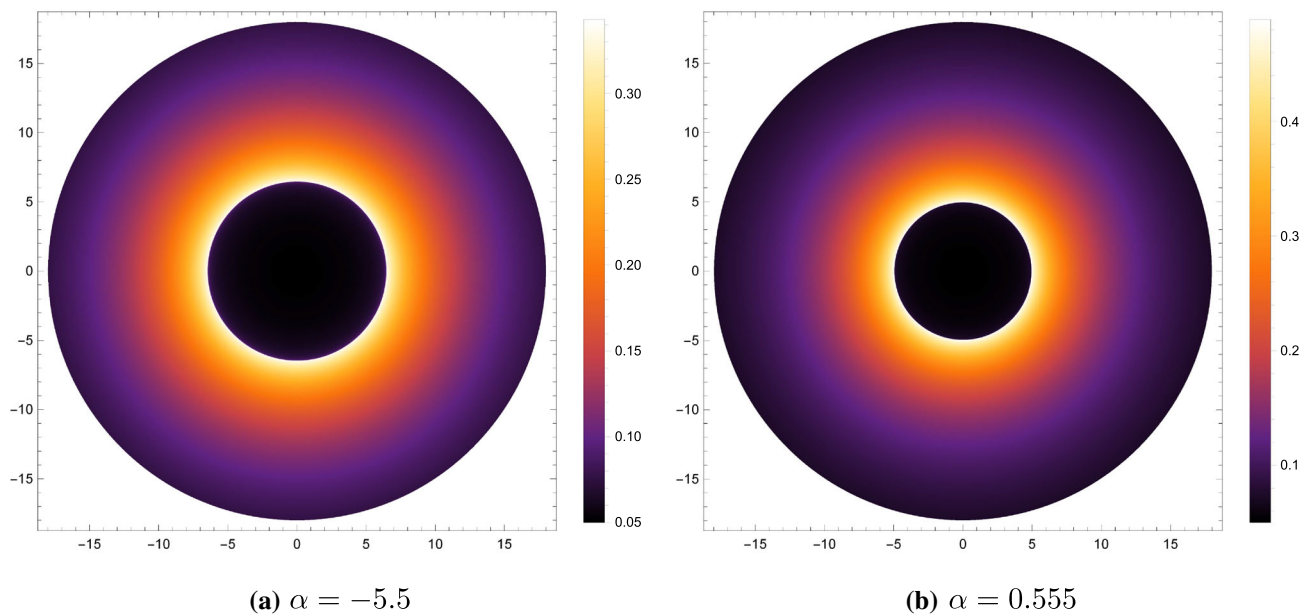**(a)** $\alpha = -5.5$ **(b)** $\alpha = 0.555$

Fig. 6 The shadow of the black hole cast by the infalling accretion for different α with $M = 1$ in the (x, y) plane. The brightest ring outside the black hole is the photon sphere

$$\frac{k_r}{k_t} = \pm \frac{1}{F(r)} \sqrt{1 - \frac{b^2 F(r)}{r^2}}, \tag{23}$$

where the sign $+ (-)$ corresponds to the case that the photon gets close to (away from) the black hole. With this equation, the redshift factor in Eq. (21) can be simplified as

$$g = \frac{1}{u_e^t + k_r / k_e u_e^r}. \tag{24}$$

In addition, the proper distance can be defined as

$$dl_{\text{prop}} = k_\gamma u_e^\gamma \, d\lambda = \frac{k_t}{g |k_r|} dr, \tag{25}$$

where λ is the affine parameter along the photon path γ. We also assume that the specific emissivity is monochromatic; therefore, Eq. (16) can be used. The intensity in Eq. (15) thus can be expressed as

$$I(\nu_o) \propto \int_\gamma \frac{g^3 k_t \, dr}{r^2 |k_r|}. \tag{26}$$

Now we will use Eq. (26) to investigate the shadow of the black hole numerically. For different α, the intensities with respect to b observed by the distant observer are shown in Fig. 5. Similar to the static accretion, we find that, as b increases, the intensity increases first, then reaches a maximum intensity at $b = b_{ph}$, and then drops away. We can also

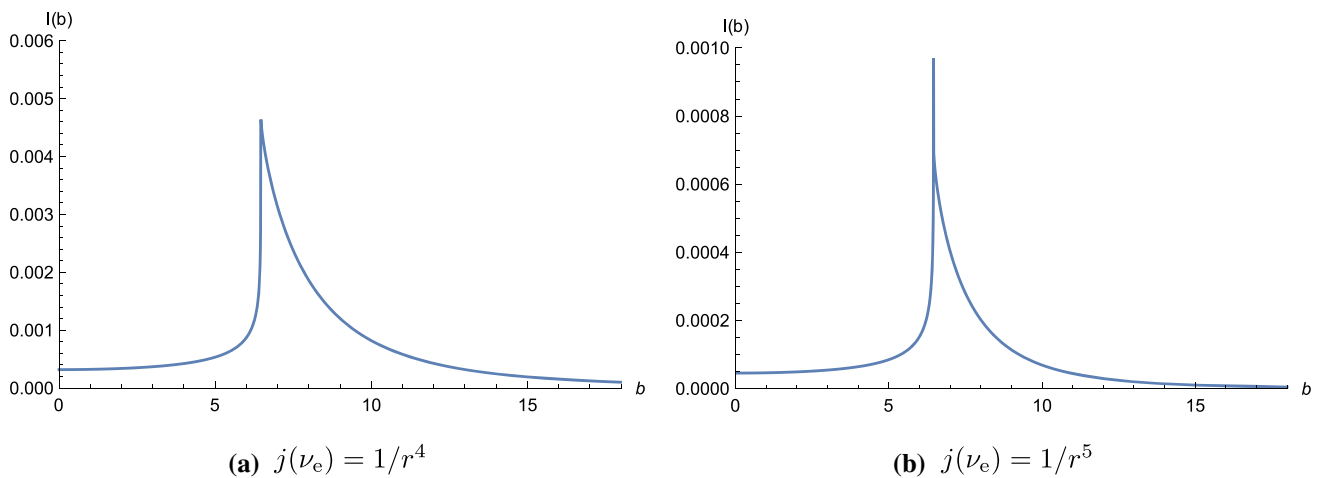**(a)** $j(\nu_e) = 1/r^4$ **(b)** $j(\nu_e) = 1/r^5$

Fig. 7 Profile of the specific intensity $I(b)$ seen by a distant observer with different profiles of specific emissivity. For both cases, we set $M = 1$, $\alpha = -5.5$
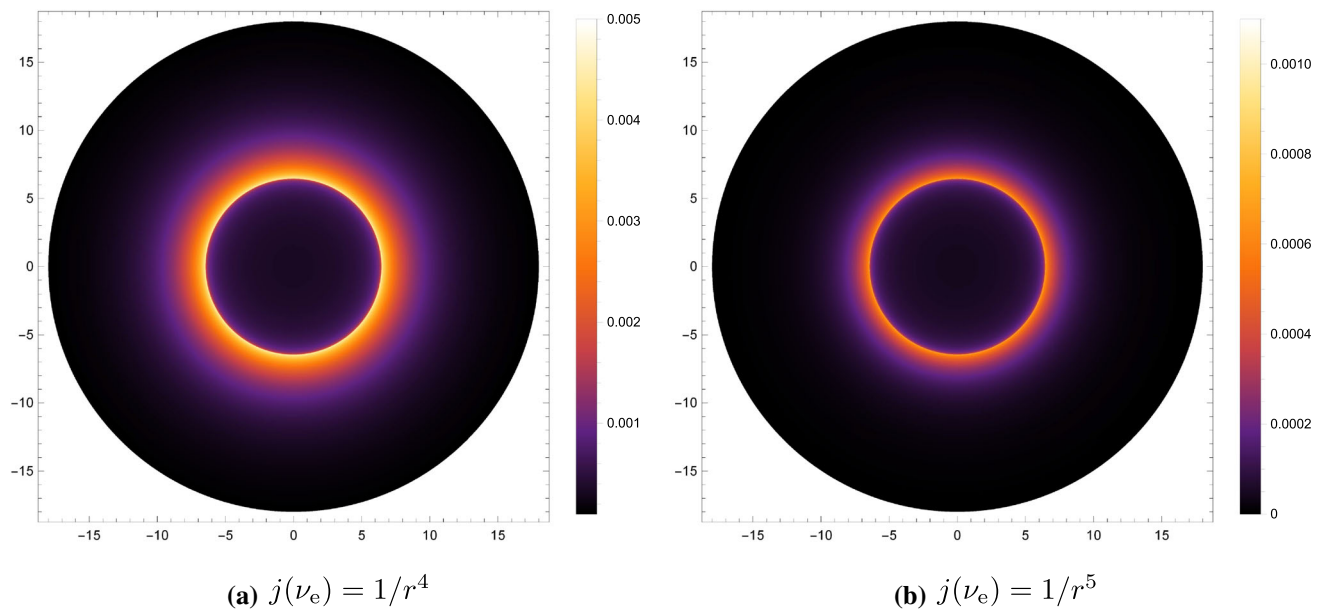

(a) $j(\nu_e) = 1/r^4$ **(b)** $j(\nu_e) = 1/r^5$

Fig. 8 The shadow of the black hole cast by the infalling accretion with different profiles of specific emissivity in the (x, y) plane. We set $\alpha = -5.5$, $M = 1$

observe the effect of α on the intensity from Fig. 5. That is, the larger the value of b is, the larger the observed intensity will be.

The two-dimensional image of the shadow and photon sphere seen by a distant observer are shown in Fig. 6. We can see that the radius of the shadow and the location of the photon sphere are the same as those with the static accretion. A major new feature is that in the central region, the shadow with infalling accretion is darker than that with the static accretion, which is well accounted for by the Doppler effect. Nearer the event horizon of the black hole, this effect is more obvious.

It has been argued that, in the universe, the accretion flows do have inward radial velocity, and the velocity tends to be

large precisely at the radii of interest for shadow formation. Therefore the model with radially infalling gas is most appropriate for comparison with the image of M87*.

In order to explore how the profile of the specific emissivity affects the shadow of the black hole, we will choose different profiles of $j(\nu_e)$. The corresponding intensities are shown in Fig. 7. From this figure, we see clearly that the intensity in these cases shows a behavior similar to the case $j(\nu_e) = 1/r^2$. That is, the peak is always located at $b = b_{ph}$. The difference is that the intensity decays faster for the higher power of $1/r$, which makes the peak more prominent. The corresponding two-dimensional images of shadow and photon sphere are shown in Fig. 8.

Our results in Figs. 7 and 8 show that although the profile of the spherical accretion affects the intensity of the shadow, it does not affect the characteristic geometry such as the radius of the shadow, which is determined only by the geometry of the spacetime.

5 Discussions and conclusions

In this paper, we have investigated the shadows and photon spheres cast by the four-dimensional Gauss–Bonnet black hole with spherical accretions. We first obtain the radius of the photon sphere and critical impact parameter for different Gauss–Bonnet constants, and find that the larger the Gauss–Bonnet constant is, the smaller the radius of the photon sphere and critical impact parameter will be, which is consistent with the previous results [50,51]. It should be noted that a simple approximation of the radius of the shadow was derived in Section 5 of [32], in which the authors mainly studied the quasi-normal modes and stability of the four-dimensional spherical Gauss–Bonnet black hole. In the concise Section 5 of [32] the authors analytically obtained a linear relation between the Gauss–Bonnet constant α with respect to the radius of the shadow, in the units of event horizon. This linear relation indeed was only satisfied in the small α regime. In fact, from the numerics in Table 1 in our paper we can check that in the units of the event horizon, the radius of the shadow also increases as α grows. However, for larger α's this linear relation will be destroyed. Therefore, our numerical evaluations actually go beyond the simple derivations in [32].

More importantly, we obtain the specific intensity $I(\nu_o)$ observed by a distant observer, in which the accretion was supposed to be either static or infalling. For both cases, we find that the specific intensity increases with the increasing Gauss–Bonnet constant. We plot the image of the shadows in the (x, y) plane, and find that there is a bright sphere ring outside the dark region. The interior region of the shadow with the infalling accretion turns out to be darker than that with the static accretion, due to the Doppler effect. We also investigate the effect of the profile of the accretion on the shadow. As a result, it is found that although the profile will affect the intensity of the shadow, it does not affect the characteristic of the geometry such as the radius of the photon sphere. In Ref. [22], the emission originating from the accretion was cut off at different locations; the size of the shadow was found to be independent of the locations. Obviously, our result is consistent with the observation in Ref. [22].

The EHT Collaboration has modeled M87* with the Kerr black hole, and claimed that the observation supports general relativity. In this paper, we did not consider the Kerr-like black hole in the four-dimensional Gauss–Bonnet gravity since the spherically symmetric black hole, in some cases, may produce qualitatively similar results [53]. For example,
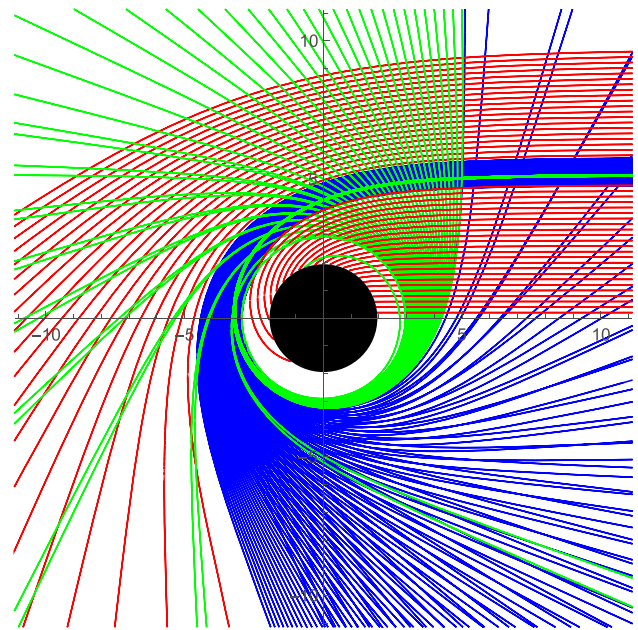

Fig. 9 The behavior of light rays as a function of the impact parameter b. We treat (r, ϕ) as the Euclidean polar coordinates. The red lines, blue lines and green lines correspond to the direct, lensed, and photon ring trajectories, respectively. The spacing in impact parameter is $1/5$, $1/100$, $1/1000$ in the direct, lensed, and photon ring bands. The black hole is shown as a solid disk and the photon orbit as a dashed line. We set $\alpha = -5.5$, $M = 1$

the simplified spherical model captures the key features that also appear in state of the art general-relativistic magnetohydrodynamics models [5], whether they are spinning or not.

In addition, the real accretion flows are generically not spherically symmetric. The hot accretion flow in M87* and most other galactic nuclei consists of a geometrically thick and quasi-spherical disk. It will be more interesting to investigate the shadow with a thick disk accretion. Recently, Ref. [21] has investigated the shadow with thin and thick accretion. They reanalyzed the orbit of photon and redefined the photon ring and lensing ring, in which the lensing ring is the light ray that intersects the plane of the disk twice and the photon ring is the one that intersects the plane three or more times. They defined a total number of orbits as $n \equiv \phi/2\pi$. In this case, $n > 3/4$ corresponds to the light ray crossing the equatorial plane at least twice, $n > 5/4$ corresponds to the light ray crossing the equatorial plane at least three times, and $n < 3/4$ corresponds to the light ray crossing the equatorial plane only once. For the case of $\alpha = -5.5$, the trajectory of the light ray is shown in Fig. 9. Comparing it with Fig. 2, we see that the photon ring is around the photon sphere, and the lensing ring is around the photon ring. It will be interesting to investigate the shadow, photon ring, and lensing ring with a thin or thick disk in the four-dimensional Gauss–Bonnet black hole. We leave this as future work.

Data Availability Statement This manuscript has no associated data or the data will not be deposited. [Authors' comment: All the data are shown as the figures and formulae in this paper. No other associated movie or animation data.]

References

1. K. Akiyama et al., [Event Horizon Telescope Collaboration] First M87 Event Horizon Telescope results. I. The shadow of the supermassive black hole. Astrophys. J. **875**(1), L1 (2019)
2. K. Akiyama et al., [Event Horizon Telescope Collaboration, First M87 Event Horizon Telescope results. II. Array and instrumentation. Astrophys. J. **875**(1), L2 (2019)
3. K. Akiyama et al., [Event Horizon Telescope Collaboration], First M87 event horizon telescope results. III. Data processing and calibration. Astrophys. J. **875**(1), L3 (2019)
4. K. Akiyama et al., [Event Horizon Telescope Collaboration], First M87 event horizon telescope results. IV. Imaging the central supermassive black hole. Astrophys. J. **875**(1), L4 (2019)
5. K. Akiyama et al., [Event Horizon Telescope Collaboration], First M87 event horizon telescope results. V. Physical origin of the asymmetric ring. Astrophys. J. **875**(1), L5 (2019)
6. K. Akiyama et al., [Event Horizon Telescope Collaboration], First M87 event horizon telescope results. VI. The shadow and mass of the central black hole. Astrophys. J. **875**(1), L6 (2019)
7. J.L. Synge, The escape of photons from gravitationally intense stars. Mon. Not. R. Astron. Soc. **131**(3), 463 (1966). https://doi.org/10.1093/mnras/131.3.463
8. J.M. Bardeen, W.H. Press, S.A. Teukolsky, Rotating black holes: locally nonrotating frames, energy extraction, and scalar synchrotron radiation. Astrophys. J. **178**, 347 (1972)
9. S.E. Gralla, A. Lupsasca, Lensing by Kerr black holes. Phys. Rev. D **101**(4), 044031 (2020)
10. A. Allahyari, M. Khodadi, S. Vagnozzi, D.F. Mota, Magnetically charged black holes from non-linear electrodynamics and the Event Horizon Telescope. JCAP **2002**, 003 (2020)
11. P.C. Li, M. Guo, B. Chen, Shadow of a spinning black hole in an expanding universe. Phys. Rev. D **101**(8), 084041 (2020)

12. I. Banerjee, S. Chakraborty, S. SenGupta, Silhouette of M87*: a new window to peek into the world of hidden dimensions. Phys. Rev. D **101**(4), 041301 (2020)
13. S. Vagnozzi, L. Visinelli, Hunting for extra dimensions in the shadow of M87*. Phys. Rev. D **100**(2), 024020 (2019)
14. S. Vagnozzi, C. Bambi, L. Visinelli, Concerns regarding the use of black hole shadows as standard rulers. Class. Quantum Grav. **37**(8), 087001 (2020)
15. M. Safarzadeh, A. Loeb, M. Reid, Constraining a black hole companion for M87* through imaging by the Event Horizon Telescope. Mon. Not. R. Astron. Soc. **488**(1), L90 (2019)
16. H. Davoudiasl, P.B. Denton, Ultralight boson dark matter and Event Horizon Telescope observations of M87*. Phys. Rev. Lett. **123**(2), 021102 (2019)
17. R. Roy, U.A. Yajnik, Evolution of black hole shadow in the presence of ultralight bosons. Phys. Lett. B **803**, 135284 (2020)
18. Y. Chen, J. Shu, X. Xue, Q. Yuan, Y. Zhao, Probing axions with Event Horizon Telescope polarimetric measurements. Phys. Rev. Lett. **124**(6), 061102 (2020)
19. J.-P. Luminet, Image of a spherical black hole with thin accretion disk. Astron. Astrophys. **75**, 228 (1979)
20. P.V.P. Cunha, N.A. Eiró, C.A.R. Herdeiro, J.P.S. Lemos, Lensing and shadow of a black hole surrounded by a heavy accretion disk. JCAP **2003**(03), 035 (2020)
21. S.E. Gralla, D.E. Holz, R.M. Wald, Black hole shadows, photon rings, and lensing rings. Phys. Rev. D **100**(2), 024018 (2019)
22. R. Narayan, M.D. Johnson, C.F. Gammie, The shadow of a spherically accreting black hole. Astrophys. J. **885**(2), L33 (2019)
23. H. Falcke, F. Melia, E. Agol, Viewing the shadow of the black hole at the galactic center. Astrophys. J. **528**, L13 (2000)
24. D. Glavan, C. Lin, Einstein–Gauss–Bonnet gravity in 4-dimensional space-time. Phys. Rev. Lett. **124**(8), 081301 (2020)
25. R.G. Cai, Gauss–Bonnet black holes in AdS spaces. Phys. Rev. D **65**, 084014 (2002)
26. D.G. Boulware, S. Deser, String generated gravity models. Phys. Rev. Lett. **55**, 2656 (1985)
27. R.A. Hennigar, D. Kubiznak, R.B. Mann, C. Pollack, On taking the $D \rightarrow 4$ limit of Gauss–Bonnet gravity: theory and solutions. arXiv:2004.09472 [gr-qc]
28. S.X. Tian, Z.H. Zhu, Comment on "Einstein–Gauss–Bonnet gravity in four-dimensional spacetime". arXiv:2004.09954 [gr-qc]
29. F.W. Shu, Vacua in novel 4D Einstein-Gauss-Bonnet Gravity: pathology and instability?. arXiv:2004.09339 [gr-qc]
30. S. Mahapatra, A note on the total action of 4D Gauss–Bonnet theory. arXiv:2004.09214 [gr-qc]
31. K. Aoki, M.A. Gorji, S. Mukohyama, A consistent theory of $D \rightarrow 4$ Einstein–Gauss–Bonnet gravity. arXiv:2005.03859 [gr-qc]
32. R.A. Konoplya, A.F. Zinhailo, Quasinormal modes, stability and shadows of a black hole in the novel 4D Einstein–Gauss–Bonnet gravity. arXiv:2003.01188 [gr-qc]
33. R.A. Konoplya, A.F. Zinhailo, Grey-body factors and Hawking radiation of black holes in 4D Einstein–Gauss–Bonnet gravity. arXiv:2004.02248 [gr-qc]
34. S.L. Li, P. Wu, H. Yu, Stability of the Einstein static universe in 4D Gauss–Bonnet gravity. arXiv:2004.02080 [gr-qc]
35. A.K. Mishra, Quasinormal modes and Strong Cosmic Censorship in the novel 4D Einstein–Gauss-Bonnet gravity. arXiv:2004.01243 [gr-qc]
36. C.Y. Zhang, P.C. Li, M. Guo, Greybody factor and power spectra of the Hawking radiation in the novel 4D Einstein–Gauss–Bonnet de-Sitter gravity. arXiv:2003.13068 [hep-th]
37. H. Lu, Y. Pang, Horndeski gravity as $D \rightarrow 4$ limit of Gauss–Bonnet. arXiv:2003.11552 [gr-qc]
38. Y.P. Zhang, S.W. Wei, Y.X. Liu, Spinning test particle in four-dimensional Einstein–Gauss–Bonnet black hole. arXiv:2003.10960 [gr-qc]

39. R.A. Konoplya, A. Zhidenko, Black holes in the four-dimensional Einstein–Lovelock gravity. Phys. Rev. D **101**, 084038 (2020)

40. P.G.S. Fernandes, Charged black holes in AdS spaces in 4D Einstein Gauss–Bonnet gravity. arXiv:2003.05491 [gr-qc]

41. P. Liu, C. Niu , C.Y. Zhang, Instability of the novel 4D charged Einstein–Gauss–Bonnet de-Sitter black hole. arXiv:2004.10620 [gr-qc]

42. S.A. Hosseini Mansoori, Thermodynamic geometry of novel 4-D Gauss Bonnet AdS black hole. arXiv:2003.13382 [gr-qc]

43. R. Roy , S. Chakrabarti, A study on black hole shadows in asymptotically de Sitter spacetimes. arXiv:2003.14107 [gr-qc]

44. D.V. Singh, S. Siwach, Thermodynamics and P-v criticality of Bardeen-AdS black hole in 4-D Einstein–Gauss–Bonnet gravity. arXiv:2003.11754 [gr-qc]

45. A. Aragón, R.Bécar, P.A. González, Y. Vásquez, Perturbative and nonperturbative quasinormal modes of 4D Einstein–Gauss–Bonnet black holes. arXiv:2004.05632 [gr-qc]

46. R. Kumar, S.G. Ghosh, Rotating black holes in the novel 4*D* Einstein–Gauss–Bonnet gravity. arXiv:2003.08927 [gr-qc]

47. X.X. Zeng, H.Q. Zhang, Influence of quintessence dark energy on the shadow of black hole. arXiv:2007.06333 [gr-qc]

48. S.U. Islam, R. Kumar, S.G. Ghosh, Gravitational lensing by black holes in 4D Einstein–Gauss–Bonnet gravity. arXiv:2004.01038 [gr-qc]

49. X.H. Jin, Y.X. Gao, D.J. Liu, Strong gravitational lensing of a 4-dimensional Einstein–Gauss–Bonnet black hole in homogeneous plasma. arXiv:2004.02261 [gr-qc]

50. M. Guo, P.C. Li, The innermost stable circular orbit and shadow in the novel 4*D* Einstein–Gauss–Bonnet gravity. arXiv:2003.02523 [gr-qc]

51. S.W. Wei, Y.X. Liu, Testing the nature of Gauss-Bonnet gravity by four-dimensional rotating black hole shadow. arXiv:2003.07769 [gr-qc]

52. R.G. Cai, L.M. Cao, N. Ohta, Black holes in gravity with conformal anomaly and logarithmic term in black hole entropy. JHEP **1004**, 082 (2010)

53. M. Jaroszynski, A. Kurpiewski, Optics near Kerr black holes: spectra of advection dominated accretion flows. Astron. Astrophys. **326**, 419 (1997)

54. C. Bambi, Can the supermassive objects at the centers of galaxies be traversable wormholes? The first test of strong gravity for mm/sub-mm very long baseline interferometry facilities. Phys. Rev. D **87**, 107501 (2013)